

X-Ray Diffraction Characterization of Crystallinity and Phase Composition in Manganese Oxides Composite Prepared by Molten Salts

Mohd Faiz Hassan*, Chan Kok Sheng

Faculty of Science and Marine Environment, Universiti Malaysia Terengganu
21030 Kuala Nerus, Terengganu, Malaysia

*Corresponding author e-mail: mfhasan@umt.edu.my

Received: 12 February 2019

Accepted: 23 April 2019

Published: 19 June 2019

ABSTRACT

The manganese oxides composite was synthesised via a simple molten salts method using a purchased $MnCl_2 \cdot 2H_2O$ as structuring agent. The structural details of the sample are important to be studied and previously rarely reported. It was characterised using X-ray diffraction (XRD) and data analyses including fitting process were done by Search-Match and Origin software. The Vesta software was used to draw a diagram crystal structure of the as-prepared composite. The experimental results indicated that the composite has two phases, Mn_3O_4 and MnO_2 , in value of approximately 74.22% and 25.78%, separately. The composite was highly crystalline with 74.69% compared to 25.31% for amorphous. The crystallite size of the Mn_3O_4 and MnO_2 were calculated in an average of 22 and 24 nm, respectively. However, the lattice strain of the as-prepared composite was obtained between 7.1×10^{-3} and 7.4×10^{-3} . The lattice parameters for the Mn_3O_4 compound was $a = 5.705 \text{ \AA}$ and $c = 9.473 \text{ \AA}$, whereas $a = 9.390 \text{ \AA}$, $b = 2.477 \text{ \AA}$, $c = 4.705 \text{ \AA}$ correspond to the MnO_2 compound. The obtained results concluded that the composite containing two different types of system structure (tetragonal and orthorhombic).

Keywords: X-ray diffraction, crystallite size, lattice strain, lattice parameters



Copyright© 2019 UiTM Press.
This is an open access article
under the CC BY-NC-ND license

PENERBIT
UNIVERSITI TEKNOLOGI MARA
PRESS

INTRODUCTION

Manganese oxide a promising materials and is widely used in energy fields such as supercapacitor and battery due to the low cost of raw materials, and the fact that manganese is considered more environmentally friendly than other noble metal oxides [1-7]. In general, the manganese oxide exists in many structural shapes such as cubic, tetragonal, and also orthorhombic structural system [8-10] and these shapes have its identifiable characteristic and behaviours [11]. The study about structural and elementary compositions on this material is crucial in order to identify their capability and suitability in the energy storage applications. Both the crystallinity and/or the amorphous phase compositions depend upon the molten salts processing parameters and are believed to affect the performance of the device (for instance, the device in energy storage applications) when employing the material in the system [12-15]. To verify the element or phase composition in the research study, X-ray diffraction is one of the recommended techniques and aligned with what proposed by a large group of researchers in materials science [1-4, 11-16].

X-ray diffraction methods have long been applied to characterise manganese oxide and related metal oxide materials. However, the quantitative phase analysis methods described to date for manganese composite has usually been developed to measure simple features of the diffraction patterns, such as crystallinity or phase content, rather than providing complete phase analysis. The simple fitting technique and the lattice strain parameters are another issues that are not or rarely addressed, make the results are insufficiently available as the reference information for the researchers to identify the appropriate materials for the proper applications.

The purpose of this paper is to describe an X-ray diffraction quantitative phase analysis technique applicable on the Mn oxides composite crystal including calculation of crystallinity percentage, phase, crystallite size, lattice strain, and lattice parameters via the analysing the XRD data by using the Search-Match, Origin and Vesta software.

EXPERIMENTAL DETAILS

The composite was prepared using lithium nitrate (LiNO_3 , 99%), lithium hydroxide monohydrate ($\text{LiOH}\cdot\text{H}_2\text{O}$, 99%), hydrogen peroxide (H_2O_2 , 32%), and manganese chloride ($\text{MnCl}_2\cdot 2\text{H}_2\text{O}$, 98%). All chemicals were purchased from Sigma Aldrich Chemical Reagent Company and used without further purification.

The starting precursors for the composite sample were weighed as follow: 1.72 g (100 mmol) of LiNO_3 , 0.21 g (20 mmol) of $\text{LiOH}\cdot\text{H}_2\text{O}$, and 0.40 g (10 mmol) of $\text{MnCl}_2\cdot 2\text{H}_2\text{O}$. The mixed precursor was mechanically ground until it is literally homogeneous. An amount of 1.42 g (50 mmol) of H_2O_2 was dropped cautiously under a fume hood and stirred for a few minutes. The mixture was transferred in a beaker and dried at 100°C for 24 hours in a vacuum oven and further heated at 300°C for three hours in a muffle furnace. The beaker was cooled down naturally before the heated sample is collected and washed for several times with distilled water and acetone using a centrifuge to remove any possible residual reactants and impurities. The product was dried in a vacuum oven at 100°C for 12 hours, giving the final as-prepared sample.

The sample phase identification, crystallinity, crystallites size, crystal structure, lattice strain and lattice parameters of the as-prepared composite were analysed using the data from X-ray diffraction (XRD) pattern. The XRD patterns of the as-prepared products were recorded on a MiniFlex II diffractometer equipped with an X'celerator using $\text{CuK}\alpha$ radiation (λ) 0.1542 nm, operated at 30 kV and 30 mA in the 2θ range between 10° and 70° . The obtained data were analysed by using Search-Match, Origin and Vesta software to confirm the reliable information of the composite.

In order to investigate the phase of the composite, the d-spacing and the intensity of peaks were determined using the Search-Match by matching the peaks of standard minerals in the given database. The crystallinity of the composite was verified using the XRD data which fitted first using the Origin software. In general, the crystallinity was evaluated by dividing the area under all peaks with the area under the whole diffractogram. The percentage of phases and crystallinity of studied composite were calculated using the eq. (1) [17-19]

$$\% \text{ of phase A} = 100 \times \frac{A_{\text{phase A}}}{A_{\text{phase A}} + A_{\text{phase B}}} \quad (1)$$

Where $A_{\text{phase A}}$ is the area of phase A and $A_{\text{phase B}}$ is the area of phase B.

In the estimation of crystallite size, the Scherrer length was calculated using the eq. (2) [19-22]

$$L = \frac{0.9\lambda}{B \cos \theta_B} \quad (2)$$

Here, λ is the wavelength of X-rays, B is the broadening line in radians at FWHM of the peak, and θ_B is the glancing angle. The Scherrer length was calculated from a few peaks, and the average value from it was taken as the final result.

The lattice strain is one of the factors which give the defect of the diffractogram and it essentials to be counted in the analysis of XRD data with the aim to reduce the imperfection of the pattern and this parameter is calculated by using Eq. (3) [20-25]

$$\varepsilon = B \times \frac{\cos \theta_B}{\sin \theta_B} \quad (3)$$

Where B is the FWHM of the peak and θ is the Bragg angle.

The last part is to determine the lattice parameters of the as-prepared composite. This data is very beneficial in order to draw the diagram of the crystal structure of composite. The lattice parameters were calculated involving the Bragg's law equation and two plane spacing equations (the tetragonal system and the orthorhombic system structures);

The Bragg's law equation (4) can be found as follows [26-28]:

$$\lambda = 2d \sin \theta \quad (4)$$

Here, λ is the wavelength of X-rays, d is the d-spacing at specified peaks, and θ is the glancing angle.

For the tetragonal system structure, the equation (5) [29] is

$$\frac{1}{d_{hkl}^2} = [h^2 + k^2 + l^2 \left(\frac{a}{c}\right)^2] \frac{1}{a^2} \quad (5)$$

The orthorhombic system structure equation (6) is similar to [29], and its expression as follows:

$$\frac{1}{d_{hkl}^2} = \frac{h^2}{a^2} + \frac{k^2}{b^2} + \frac{l^2}{c^2} \quad (6)$$

Where, d_{hkl} is the d-spacing at specified hkl plane, a , b and c are the lattice constants or parameters which can be determined by X-ray diffractogram (XRD).

RESULTS AND DISCUSSION

Figure 1 shows the X-ray diffractograms of Mn₃O₄-MnO₂ composite, before (a) and after (b) fitted process. The diffractogram indicates a high crystalline structure and is identified as the combination of two phases, Mn₃O₄ and MnO₂. The first phase can be indexed to the Mn₃O₄, hausmannite structure (space group I41/amd) (JCPDS 02-1062). The Mn₃O₄ peaks can be noticed at $2\theta = 29.34, 31.36, 32.68, 36.57, 37.99, 44.83, 51.03, 56.34, 58.97$ and 64.97° which can be assigned to the (112), (200), (103), (211), (004), (220), (105), (303), (321), and (314) planes, and is a well agreement with a tetragonal structure with lattice constants of $a = 5.75 \text{ \AA}$ and $c = 9.42 \text{ \AA}$, respectively. The second phase is corresponding to the MnO₂, ramsdellite structure (space group Pnma) (JCPDS 42-1316). The peaks of MnO₂ are observed at $2\theta = 18.90, 21.23, 48.40$ and 68.03° which consigned to the (200), (101), (302), and (610) planes, and is a well arrangement with an orthorhombic structure with lattice constants of $a = 9.39 \text{ \AA}$, $b = 2.47 \text{ \AA}$ and $c = 4.71 \text{ \AA}$. The pattern is also similar to [31], who studies on a similar type of compound.

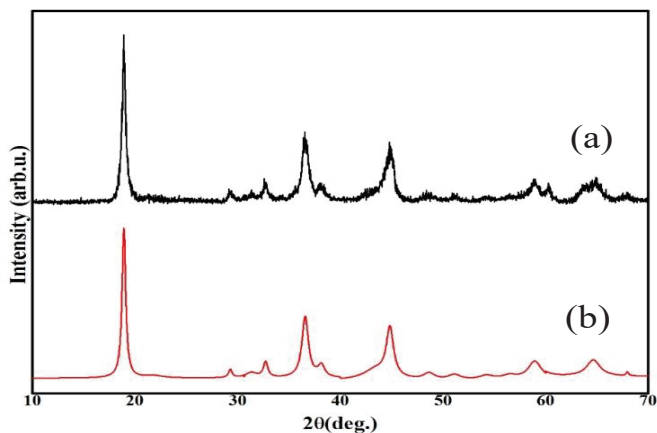


Figure 1: XRD Patterns for an As-Prepared Compound: (a) Before and (b) After Fitted

The d-spacing value for the respective peaks for both phases is tabulated in Table 1. The values for individual peak were identified by using a Search-Match software and compared them with the provided data from the databank of the software. From the result, it can be seen that the d-spacing values of Mn_3O_4 and MnO_2 phases are almost well-matched to the specified values in the JCPDS database which it can be confirmed that the analysed sample was the combination of Mn_3O_4 and MnO_2 phases.

Table 1: The d-Spacing Values of the Respective Peaks for Mn_3O_4 and MnO_2 Phases Compound

Peak	Mn_3O_4		
	Current Study		JCPDS 02-1062
	2θ (°)	d (Å)	d (Å)
P1	29.34	3.04	3.09
P2	31.36	2.85	2.87
P3	32.68	2.74	2.75
P4	36.57	2.46	2.48
P5	37.99	2.37	2.35
P6	42.46	2.12	2.12

P7	44.83	2.02	2.03
P8	51.03	1.79	1.79
P9	54.24	1.69	1.69
P10	56.34	1.63	1.64
P11	58.97	1.56	1.57
P12	64.97	1.43	1.44

MnO ₂			
Peak	Current Study		JCPDS 42-1316
	2 θ (°)	d (Å)	d (Å)
PK1	18.9	4.68	4.76
PK2	21.23	4.16	4.21
PK3	48.4	1.88	1.89
PK4	68.03	1.38	1.39

Figure 2 shows area for the individual peak ((a) Mn₃O₄ and (b) MnO₂) calculated from the fitted XRD pattern (see Figure 1(b)). The fitting proses were performed using the Origin software and the area for every phase was calculated based on the area underneath of peaks that has high intensity. The total area of Mn₃O₄ peaks was estimated around 1180.21 units², while for MnO₂ the expectable values were at 409.91 units². These areas are also recognised as the crystalline phase and counted in the calculation to obtain the percentage of crystallinity/amorphous state of the composite.

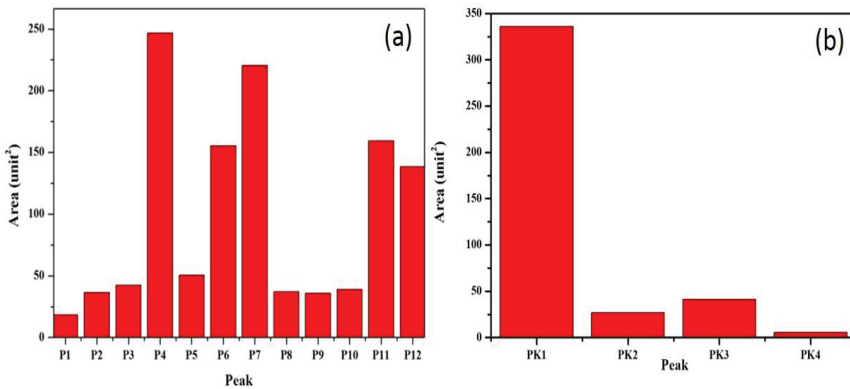


Figure 2: The Graph Area versus Peak for (a) Mn₃O₄ and (b) MnO₂

The specific information of $\text{Mn}_3\text{O}_4\text{-MnO}_2$ composite including of area for the respective phase, baseline, and percentage of crystallinity/amorphous and percentage for every compound is organised in Table 2. As mentioned earlier, the area underneath of the peaks are considered as the crystalline structure which gives the total area of 1590.12 units² and for the amorphous structure, its area was taken from the baseline of the diffractogram which counted to be 538.72 units². The percentages of crystallinity and amorphous were calculated by using the Eq. (1) which their values are 74.69 and 25.31%, respectively. The similar equation was also used to calculate the percentage of every phase in the sample, which give the value to be 74.22 and 25.78% for Mn_3O_4 and MnO_2 , individually.

Table 2: The Specific Information of $\text{Mn}_3\text{O}_4\text{-MnO}_2$ Sample

$\text{Mn}_3\text{O}_4\text{-MnO}_2$		
No.	Description	Value
1	Total area of Mn_3O_4 peaks (units ²)	1180.21
2	Total area of MnO_2 peaks (units ²)	409.91
3	Total area of baseline (units ²)	538.72
4	% of crystallinity	74.69
5	% of amorphousity	25.31
6	% of Mn_3O_4	74.22
7	% of MnO_2	25.78

Table 3 represents the result of the full wave at the half maximum (FWHM), B, Scherrer Length, L and Lattice Strain, θ of the as-prepared sample. The data were evaluated from the selected peaks of the fitted diffractogram (Fig. 1b). The Scherrer length for every peak was estimated by using the Eq. (2) and their average sizes were 22.5 nm and 24.4 nm for Mn_3O_4 and MnO_2 . The small size of the Scherrer length of Mn_3O_4 gives the meaning that its particle size is estimated smaller compared to the MnO_2 [33]. The lattice strain is one of the factors that contribute to the defectiveness of the XRD diffractogram of the sample [34]. In this study, the obtained peaks face the phenomenon where the plotted peaks shifted to lower or higher angles (peak moves or broaden) as analysed using the eq. (3). This occurred shifting, most probably due to the heating process with

different temperatures as stated in the experimental section. From Table 3, the average lattice strain for Mn_3O_4 and MnO_2 phases are in between 7.2×10^{-3} and 7.4×10^{-3} .

Table 3: The FWHM, Scherrer Length and Lattice Strain Information of the As-Prepared Sample

Mn_3O_4					
Peak	(hkl)	2θ (°)	FWHM,B (rad)	L (nm)	Lattice Strain
P1	112	29.34	0.006	45.3	0.006
P3	103	32.68	0.007	24.6	0.006
P4	211	36.57	0.011	15.4	0.008
P7	220	44.83	0.011	14.1	0.007
P11	321	58.97	0.019	21.0	0.008
P13	314	64.97	0.020	14.3	0.008
MnO_2					
Peak	(hkl)	2θ (°)	FWHM,B (rad)	L (nm)	Lattice Strain
PK1	200	18.9	0.007	19.8	0.011
PK3	302	48.4	0.016	14.7	0.009
PK4	610	68.03	0.004	38.5	0.002

The as-prepared composite has successfully investigated having Mn_3O_4 and MnO_2 phases with tetragonal and orthorhombic system structures. Their lattice constants can be obtained from the Eq. (4), (5) and (6). For the tetragonal system, the lattice constant must follow the rule of $a = b \neq c$. From the Bragg's law (Eq. 4), it can be re-write as $\sin 2\theta = \lambda/2d$ and combined with the plane spacing equation (Eq. 5), the lattice constants for the system will be $a = b = 5.71 \text{ \AA}$ and $c = 9.42 \text{ \AA}$. The lattice constant for the orthorhombic system was calculated using a similar concept by combining the transformed Bragg's law equation with Eq. (6) and follows the law of $a \neq b \neq c$. The lattice constants for this system were $a = 9.39 \text{ \AA}$, $b = 2.48 \text{ \AA}$, and $c = 4.71 \text{ \AA}$. The values are in good agreement with the values provided in the JCDPS database for both systems. These lattice constant parameters were used to draw a diagram to represent the crystal structure of the as-prepared composite as depicted in Figure 3. As can be seen on hausmannite (Mn_3O_4), for each manganese atom, its linkage to four oxygen atoms, while for ramsdellite (MnO_2), each manganese atom is bond to six oxygen atoms and also link to another manganese atom as well.

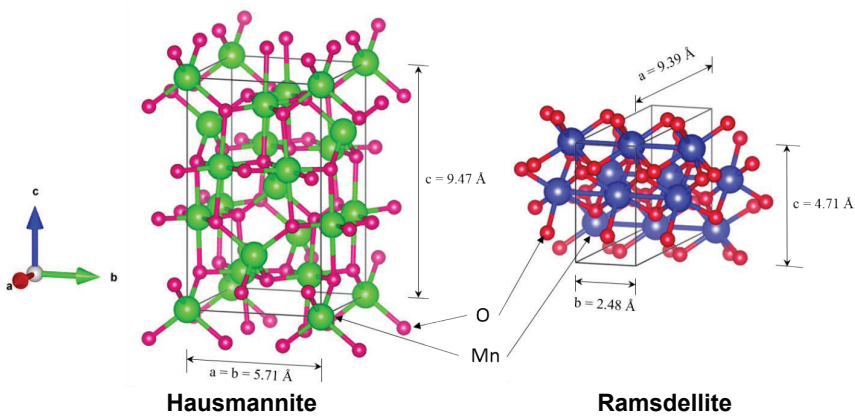


Figure 3: A Diagram of the Crystal Structure of the Different Phases in the Synthesised Sample

CONCLUSION

This present work provides the useful information of as-prepared Mn_3O_4 - MnO_2 composite specifically on its elementary phase, amorphousness/crystallinity and lattice parameters identifications using an undisruptive technique. Based on modest approaches of XRD analysis, the as-prepared composite can be confirmed containing 74.22% and 25.78% of Mn_3O_4 and MnO_2 compounds, respectively. The sample also is dominated by crystalline phase with a percentage of 74.69%. From the calculated lattice parameters, phases of as-prepared composite tended close to be tetragonal and orthorhombic system structures.



REFERENCES

- [1] C.Y. Chen, C.K. Lin, M.H. Tsai, C.Y. Tsay, P.Y. Lee, G.S. Chen, 2008. Characterization of nanocrystalline manganese oxide powder prepared by inert gas condensation, *Ceramics International*, 34, pp. 1661-1666. Doi: 10.1016/j.ceramint.2007.05.013.
- [2] J.N. Broughton, M.J. Brett, 2004. Investigation of thin sputtered Mn films for electrochemical capacitors, *Electrochimica Acta*, 49(25), pp. 4439-4446. Doi: 10.1016/j.electacta.2004.04.035.
- [3] B. Djurfors, J.N. Broughton, M.J. Brett, D.G. Ivey, 2003. Microstructural characterization of porous manganese thin films for electrochemical supercapacitor applications, *Journal of Materials Science*, 38, pp. 4817-4830. Doi: 10.1023/B:JMSE.0000004401.81145.b6.
- [4] Y.S. Chen, C.C. Hu, Y.T. Wu, 2004. Capacitive and textural characteristics of manganese oxide prepared by anodic deposition: effects of manganese precursors and oxide thickness, *Journal of Solid State Electrochemistry*, 8, pp. 467-473. Doi: 10.1007/s10008-004-0500-6.
- [5] J. Gu, X. Fan, X. Liu, S. Li, Z. Wang, S. Tang, D. Yuan, 2017. Mesoporous manganese oxide with large specific surface area for high-performance asymmetric supercapacitor with enhanced cycling stability, *Chemical Engineering Journal*, 324, pp. 35-43. Doi: <https://doi.org/10.1016/j.cej.2017.05.014>.
- [6] N. Zhang, F. Cheng, J. Liu, L. Wang, X. Long, X. Liu, F. Li & J. Chen, 2017. Rechargeable aqueous zinc-manganese dioxide batteries with high energy and power densities, *Nature Communications*, 8, Article number: 405. Doi: <https://doi.org/10.1038/s41467-017-00467-x>.
- [7] C. Ling and R. Zhang, 2017. Manganese dioxide as rechargeable magnesium battery cathode, *Frontiers in Energy Research*, 5, Article number: 30. Doi: <https://doi.org/10.3389/fenrg.2017.00030>.



- [8] R. Tsybukh, 2010. A comparative study of platinum nanodeposits on HOPG (0001), MnO(100) and MnOx/MnO(100) surfaces by STM and AFM after heat treatment in UHV, O₂, CO and H₂, Unpublished Ph.D. thesis, Universiteit Leiden, Leiden. Doi: <http://hdl.handle.net/1887/15973>
- [9] A.H. Al-Falahi, 2013. Structural and optical properties of MnO₂: Pb Nanocrystalline thin films deposited by chemical spray pyrolysis, *IOSR Journal of Engineering*, 3, pp. 52-57.
- [10] G. V. Bazueva, A. P. Tyutyunnik, A. V. Korolevb, E. Suard, C. Tai and N. V. Tarakina, 2019. The effect of manganese oxidation state on antiferromagnetic order in SrMn_{1-x}SbxO₃ (0 < x < 0.5) perovskite solid solutions, *Journal of Materials Chemistry C*, 7, pp. 2085-2095. Doi: 10.1039/c8tc05717f.
- [11] J.E. Post, 1999. Manganese oxide minerals: Crystal structures and economic and environmental significance. In *Proceedings of the National Academy of Sciences of the United State America*, 96(7), pp. 3447-3454. Doi: 10.1073/pnas.96.7.3447.
- [12] M. Sun, B. Lan, L. Yu, F. Ye, W. Song, J. He, G. Diao, Y. Zheng, 2012. Manganese oxides with different crystalline structures: Facile hydrothermal synthesis and catalytic activities, *Materials Letters*, 86, pp. 18-20. Doi: [dx.doi.org/10.1016/j.matlet.2012.07.011](https://doi.org/10.1016/j.matlet.2012.07.011).
- [13] S. Devaraj, N. Munichandraiah, 2008. Effect of crystallographic structure of MnO₂ on its electrochemical capacitance properties, *The Journal of Physical Chemistry C*, 112, pp. 4406-4417. Doi: 10.1021/jp7108785.
- [14] O. Ghodbane, J.L. Pascal, F. Favier, 2009. Microstructural effects on charge-storage properties in MnO₂-based electrochemical supercapacitors, *ACS Applied Materials and Interfaces*, 1(5), pp. 1130-1139. Doi: 10.1021/am900094e.

- [15] F. Cheng, Y. Su, J. Liang, Z. Tao, J. Chen, 2010. MnO₂-Based nanostructures as catalysts for electrochemical oxygen reduction in alkaline media, *Chemistry Materials*, 22, pp. 898-905. Doi: 10.1021/cm901698s.
- [16] S. Jucha, G. Moskal, M. Mikuśkiewicz, M. Stopyra, 2016. XRD study of Eu₂O₃-ZrO₂ feedstock powders and sintered materials, *Acta Physica Polonica A*, 130, pp. 866-905. Doi: 10.12693/APhysPolA.130.866.
- [17] Cláudia T. Kniess, João Cardoso de Lima and Patrícia B. Prates (March 23rd 2012). The Quantification of Crystalline Phases in Materials: Applications of Rietveld Method, Sintering - Methods and Products, Volodymyr Shatokha, IntechOpen. Doi: 10.5772/34400. Available from: <https://www.intechopen.com/books/sintering-methods-and-products/the-quantification-of-crystalline-phases-in-materials-applications-of-rietveld-method>
- [18] P.S. Prevey, 2000. X-ray diffraction characterization of crystallinity and phase composition in plasma-sprayed hydroxyapatite coatings, *Journal of Thermal Spray Technology*, 9(3), pp. 369-376. Doi: 10.1361/105996300770349827.
- [19] M.F. Hassan and A.K. Arof, 2005. Ionic conductivity in PEO-KOH polymer electrolytes and electrochemical cell performance, *Physica Statue Solidi A*, 202(13), pp. 2494-2500. Doi: 10.1002/pssa.200521188.
- [20] A. Monshi, M. R. Foroughi, M. R. Monshi, 2012. Modified Scherer equation to estimate more accurately nano-crystallite size using XRD, *World Journal of Nano Science and Engineering*, 2(3), pp. 154-160. Doi: 10.4236/wjnse.2012.23020.
- [21] B.R. Rehani, P.B. Joshi, N.L. Kirit and A. Pratap, 2006. Crystallite size estimation of elemental and composite silver nano-powders using XRD principles, *Indian Journal of Pure & Applied Physics*, 44(2), pp. 157-161. Doi: <http://nopr.niscair.res.in/handle/123456789/8253>.

- [22] E. Purushotham, N. Krishna, 2013. X-ray determination of crystallite size and effect of lattice strain on Debye–Waller factors of platinum nano powders, *Bulletin of Materials Science*, 36(6), pp. 973-976. Doi: 10.1007/s12034-013-0553-1.
- [23] C. Melis, L. Colombo, G. Mana, 2015. Lattice strain at c-Si surfaces: a density functional theory calculation, *Metrologia*, 52(2), pp. 1-14. Doi: 10.1088/0026-1394/52/2/214/meta.
- [24] V.D. Mote, Y. Purushotham, B.N. Dole, 2012. Williamson-Hall analysis in estimation of lattice strain in nanometer-sized ZnO particles, *Journal of Theoretical and Applied Physics*, 6, p. 6. Doi: 10.1186/2251-7235-6-6.
- [25] P. Bindu, S. Thomas, 2014. Estimation of lattice strain in ZnO nanoparticles: X-ray peak profile analysis, *Journal of Theoretical and Applied Physics*, 8, pp. 123-134. Doi: 10.1007/s40094-014-0141-9.
- [26] P. Fewster, 2014. A new theory for X-ray diffraction, *Acta Crystallographica*, A70, pp. 257-282. Doi: 10.1107/S205327331400117X.
- [27] L. Alianelli, 2002. Characterization and modelling of imperfect crystals for thermal neutron diffraction. Unpublished Ph.D. thesis, Universite Joseph Fourier, Grenoble, France.
- [28] T. Theivasanthi, M. Alagar, 2010. Preparation and characterization of near Nano copper powder by electrolytic route, *Archives of Physics Research*, 1(2), pp. 112-117.
- [29] F. Sher, 2007. Crystal Structure Determination I. In National Workshop on Crystal Structure Determination using Powder XRD, Khwarzimid Science Society, Lahore.
- [30] W. Gao, S. Ye, M. Shao, 2011. Solution-combusting preparation of mono-dispersed Mn_3O_4 nanoparticles for electrochemical applications, *Journal of Physics and Chemistry of Solids*, 72(9), pp. 1027-1031. Doi: 10.1016/j.jpcs.2011.05.015.



- [31] L.X. Yang, Y.J. Zhu, H. Tong, W.W. Wang, G.F. Cheng, 2006. Low temperature synthesis of Mn_3O_4 polyhedral nanocrystals and magnetic study, *Journal of Solid State Chemistry*, 179(4), pp. 1225-1229. Doi: 10.1016/j.jssc.2006.01.033.
- [32] S. Lee, B. Choi, N. Hamasun, C. Fushimi, A. Tsutsumi, 2008. Characterization of MnO_2 positive electrode for fuel cell/battery (FCB), *Journal of Power Sources*, 181(1), pp. 177-181. Doi: 10.1016/j.jpowsour.2008.02.083.
- [33] L. Alexander, H.P. Klug, 1950. Determination of crystallite size with the X-Ray spectrometer, *Journal of Applied Physics*, 21, p. 137. Doi: 10.1063/1.1721595.
- [34] C.R. Wie, 1994. High resolution X-ray diffraction characterization of semiconductor structures, *Materials Science and Engineering: R: Reports*, R13, p. 1. Doi: [https://doi.org/10.1016/0927-796X\(94\)90008-6](https://doi.org/10.1016/0927-796X(94)90008-6).



